Crystal Structure of the Hexameric Catabolic Ornithine Transcarbamylase from *Lactobacillus hilgardii*

Blanca de las Rivas[1], Gavin C. Fox[2], Iván Angulo[3], Martín M. Ripoll[3], Héctor Rodríguez[1], Rosario Muñoz[1] and José M. Mancheño[3]

From [1]Departamento de Microbiología, Instituto de Fermentaciones Industriales, CSIC, Juan de la Cierva 3, E-28006 Madrid, SPAIN, [2]European Synchrotron Radiation Facility, LLS-BM16, Grenoble Cedex 9, France, [3]Grupo de Cristalografía Macromolecular y Biología Estructural, Instituto Rocasolano, CSIC, Serrano 119, E-28006 Madrid, SPAIN

Running head: Hexameric catabolic OTC from *Lactobacillus hilgardii*

Address correspondence to: José M. Mancheño, Grupo de Cristalografía Macromolecular y Biología Estructural, Inst. Rocasolano, CSIC, Serrano, 119, 28006 Madrid, SPAIN. Tel: 34-915619400; Fax:34-915642431; E-mail: xjosemi@iqfr.csic.es

Catabolic ornithine transcarbamylase (cOTC; EC 2.1.3.3) catalyzes the formation of ornithine (ORN) and carbamoyl phosphate (CP) from citrulline, which constitutes the second step of the degradation of the amino acid arginine via the arginine deiminase pathway. Here, we report the crystal structure of cOTC from the lactic acid bacteria *Lactobacillus hilgardii* (Lh-cOTC) refined to 2.1 Å resolution. The structure reveals that Lh-cOTC forms a hexameric assembly, which was also confirmed by gel-filtration chromatography and analytical ultracentrifugation. The homohexamer, with 32 point group symmetry, represents a new oligomeric state within the members of the OTC family which are typically homotrimeric or homododecameric. The C-terminal end from each subunit comprises a key structural element for the stabilization of the hexameric assembly in solution. Additionally, the structure also reveals for the first time in the OTC family a metal binding site located at the three-fold molecular symmetry axis of each trimer. The bound metal has been identified as a nickel ion which is octahedrically coordinated to local symmetry-related histidine side chains and to three ordered water molecules.

Catabolic ornithine transcarbamylases (cOTC; EC 2.1.3.3) participate in the degradation of the amino acid arginine via the deiminase pathway by catalyzing the formation of ornithine (ORN) and carbamoylphosphate (CP) from citrulline. Although thermodynamically unfavored (1), this chemical reaction is exploited by a number of microorganisms which degrade arginine because of the coupling with carbamate kinase (CK), which catalyzes the next downstream step in the catabolic deiminase pathway and, in the case of cOTC from *P. aeruginosa*, because of its low affinity towards CP and its strong co-operativity for this substrate (2-6). Regulation of the enzymatic activity of cOTC from *P. aeruginosa* is highly complex. As well as displaying homotropic co-operativity towards CP, this enzyme is allosterically activated by AMP or inorganic phosphate and inhibited by polyamines such as spermidine and putrescine (6, 7). Crystal structures of the native form of cOTC from *P. aeruginosa* (8, 9) and a point mutant variant devoid of homotropic interactions (7), represent the only previously determined structures of a catabolic OTCase. The latter structure in which Glu-105 is substituted by Gly reveals that the enzyme is composed of four trimers tetrahedrically arranged according to a 23 point-group symmetry. Importantly, the allosteric regulation exhibited by this catabolic OTCase is directly correlated to its symmetrical oligomeric structure, since modification of the trimer interfaces renders trimeric and Michaelian variants (10). Conversely, anabolic OTC´s (aOTC´s) are cyclic homotrimers which display Michaelis-Menten kinetics (6). These trimers are generally referred to as "catalytic trimers" as they constitute the basic catalytic structural unit in OTC´s and more generally amongst the carbamoyltransferases (11). Representative crystal structures of anabolic OTC´s (aOTC´s) from several sources have been determined: human aOTC complexed with the bisubstrate analog *N*-(phosphonacetyl)-L-ornithine (PALO) (12), and more recently with CP and the inhibitor L-norvaline (NVA) (13); unliganded

aOTC from *E. coli* (14) as well as complexes with PALO (15) and with N^{δ}-(*N*-sulfodiaminophosphinyl)-L-ornithine (PSORN) (16); aOTC from *Pyrococcus furiosus* (17) and, finally, aOTC from *Mycobacterium tuberculosis* both unliganded and in complex with CP and NVA (18). Interestingly, aOTC from *P. furiosus* despite being an anabolic enzyme is a dodecamer assembly (17) and shows no allosteric regulation. Specifically, the quaternary structure of this OTC has been correlated to its thermostability (17).

Here we report the crystal structure of the catabolic OTCase from *Lactobacillus hilgardii* (Lh-cOTC). The hexameric structure of Lh- cOTC exhibits a new oligomeric state within the OTCases and reveals the C-terminal end of the polypeptide chains as a key structural element in the association of the subunits. Furthermore, a metal binding site is identified in the structure at the three-fold molecular symmetry axis, providing the first structural evidence for the association between an OTC and a metal ion.

EXPERIMENTAL PROCEDURES

Site-directed Mutagenesis of Lh-cOTC- A deletion mutant of Lh-cOTC lacking the last six amino acid residues (Lh-cOTC$_{337}$) was constructed by site-directed mutagenesis PCR using the plasmid pURI3-OTC as a template (19). The mutagenic primers used to introduce a stop codon at position 338 were L338Stop-5 (5´-CAACTTTGGGTAAC**TG**ATTCATTCCTAGAG) and L338Stop-3 (5´- CTCTAGGAATGAA T**CA** GTTACCCAAAGTTG) (the nucleotide changes used to introduce the mutation are given in bold). Briefly, to introduce the amino acid change, the corresponding pair of primers was used as a homologous primer pair in a PCR reaction utilising the pURI3-OTC plasmid as template and the DNA polymerase *Pfu*. The product of the PCR was digested with *Dpn*I that exclusively restricts methylated DNA (20). *E. coli* cells were transformed directly with the digestion product. The resulting plasmid, expressing the mutated Lh-cOTC gene was then sequenced to verify that no unwanted mutations had been introduced.

Protein Expression and Purification- The cloned Lh-cOTC or Lh-cOTC$_{337}$ containing vectors were transformed into *E. coli* JM109 (DE3; pLysS) by electroporation. *E. coli* cells were grown in LB medium at 37ºC with 100 μg/ml ampicillin and 34 μg/ml chloramphenicol to midexponential phase (A_{600} = 0.6) and for an additional 20 h at 22ºC after adding 0.4 mM isopropyl 1-thio-β-D-galactopyranoside to induce expression. Expressed wild-type protein was purified using a HisTrap FF Ni-affinity column (GE Healthcare), followed by a HiTrap Q HP column (GE Healthcare), and finally, a Superdex 200 prep grade column (GE Healthcare). The purified recombinant material was concentrated to 10 mg/ml in 20 mM Tris-HCl buffer (pH 8.0) containing 0.1 M NaCl. The Lh-cOTC$_{337}$ mutant was purified using a single step protocol with a HisTrap FF Ni-affinity column (GE Healthcare).

Determination of Enzyme Activity- OTC activity was determined by measuring the formation of citrulline from ornithine and carbamyl phosphate as described previously (21). Briefly, Lh-cOTC (15 ng) was incubated in a solution containing 10 mM ornithine and 50 mM EDTA (pH 8). The reaction was initiated by the addition of 10 mM carbamyl phosphate (final concentration). After 10 min at 37 ºC, the reaction was stopped with 2N HCl and the amount of citrulline formed was determined as previously described (22). One enzyme unit was taken to be the amount of enzyme needed to produce 1 μmol of citrulline per h per mg of protein.

Analytical ultracentrifugation and gel filtration- Equilibrium and sedimentation velocity ultracentrifugation experiments were performed at 10,500 rpm, 20ºC, using a Beckman XL-A ultracentrifuge with an An-50Ti rotor and standard double sector centerpiece cells. Solvent density (1.005 mg/ml) and the partial specific volume of OTC (0.736) were calculated from the buffer composition (100 mM NaCl, 20 mM Tris-HCl) and from the predicted amino acid composition, respectively, with SEDNTERP (23). Centrifugation data were analyzed using Beckman-Origin software. Gel filtration assays were carried out on Superdex 200 10/300 GL Tricorn column (GE Healthcare) using a BioRad BioLogic DuoFlow FPLC.

Data collection and processing- Trigonal Lh-cOTC crystals were produced as previously described (19). Crystals suitable for X-ray analysis were transferred to an optimized cryoprotectant solution (reservoir solution plus 20% (*v/v*) 2-methyl-2,4-pentanediol) for ~5 secs and then cryocooled at 100 K in the cold nitrogen-gas stream. Diffraction data were recorded on an ADSC Q210r CCD detector (Area Detector Systems Corp.) at beamline BM16 at the European Synchrotron Radiation Facility (ESRF) (Grenoble, France). X-ray fluorescence emission (XFE) spectra were recorded at an energy of 13 keV at beamline ID14-4 and X-ray absorption near edge

structure (XANES) spectra at beamlines BM16, ID14-4 and ID23-1 (ESRF; Grenoble, France).The measured fluorescence data were filtered and analyzed using PyMCA (24). Diffraction images were processed with MOSFLM (25) and the data scaled and analyzed using SCALA the CCP4 software suite (26). Data statistics are summarised in **Table 1**.

Structure determination and refinement- The crystal structure was determined by the molecular replacement method using the program MOLREP (27) from the CCP4 software suite (26). The atomic coordinates of cOTC from *Pseudomonas aeruginosa* (PDB code: 1dxh) were used as a search model. Initial rigid body refinement followed by several cycles of refinement with REFMAC (28), together with automatic water molecule placement with ARP/wARP (29), generated an initial model which was iteratively improved by cycles of manual rebuilding with O (30). Stereochemical validation was carried out using the program PROCHECK (31). The position of the nickel ion was determined unambiguously from a model-phased difference Fourier map at 20 σ and confirmed by an anomalous difference Fourier map generated from data collected at the Ni-peak (7.478 keV) at beamline BM16 (ESRF; Grenoble, France). The refinement statistics are summarized in **Table 1**. The final model has an R-factor of 20.3 % and an R_{free} of 24.8%, and included 1023 amino acid residues, 1 nickel ion and 191 solvent molecules. Protein models were superimposed and their root-mean-square-deviations (r.m.s.d.) were determined with the LSQKAB program (32) from the CCP4 suite (26). The PISA server from the European Bioinformatics Institute (33) was used to calculate values of buried interface areas. Ribbon diagrams were prepared using PyMOL (34).

RESULTS AND DISCUSSION

Description of the monomer structure- Each monomer of Lh-cOTC is composed of 343 amino acid residues and, as with previously described OTC´s, comprises two structurally and functionally distinct domains: the N-terminal CP-binding domain and the C-terminal ORN-binding domain. Each domain is formed by a parallel β-sheet (four- and five-stranded for the N-terminal and C-terminal sheets, respectively), which is flanked by α helices (**Fig. 1**). The secondary structural elements of Lh-cOTC together with sequence alignments against OTC´s of known 3D structure are shown in **Fig. 2**. Helices α5 (residues 141-155) and α13 (residues 316-335) constitute the interface between the domains of the Lh-cOTC monomers. The main stabilizing interactions involving these two helices are summarized in **Table S1**. Helices α5 and α13 are key structural elements as they constitute the inner core of the monomer framework and are involved in extensive interactions both between themselves and with helices α1 (residues 23-42), α2 (residues 63-75), and α6 (residues 172-184). Furthermore, α5 and α13, together with helices α2 and α6 and the connecting loop between β9-α11 (residues 278-287) make up, which is located within a cleft between the lobes of the monomer. The β9-α11 loop contains the conserved HCLP motif which participates in ornithine binding.

The three independent monomers of the asymmetric unit of the Lh-cOTC trigonal crystal superimpose almost perfectly showing a maximum r.m.s. deviation value of 0.3 Å for 343 aligned Cα atoms. Comparison of the overall topologies of the OTC´s reveals that the monomeric architecture is highly conserved with r.m.s. deviation values ranging from 1.1 Å to 1.5 Å for ~290 Cα atoms **(Table S2)**. Interestingly, the most significant structural variations are found at the N- and C-terminal segments of the proteins, which in the case of Lh-cOTC participate in hexamer formation. Finally, Lh-cOTC possesses a sequence motif characteristic of prokaryotic OTC´s (residues 283-301), which has been implicated in potential protein-protein interactions (12).

Interactions between monomers within trimers- The 3-fold cyclical arrangement of the Lh-cOTC subunits results in the formation of an indented triangular homotrimer with an approximate side-length of 90 Å and a thickness of 55 Å. The individual monomers mainly interact through their N-terminal CP-binding domains, which form the inner part of the assembly but also through the loop containing helix α11 (residues 283-301). The average value of the buried interface area between two adjacent monomers calculated by the PISA server (33) is 1065 $Å^2$. Residues involved in these intersubunit interactions mainly belong to helices α2, α11 and loop β9-α11 from one monomer and strand β1, loop β2-α3 and helix α3 from another monomer. Hydrogen bonding interactions and salt bridges identified in these interfaces are shown in **Table 2**. In addition to the salt bridge between Arg-64 and Glu-94, present in all OTC´s with known 3D structure, other salt bridges specific to Lh-cOTC include: Arg-66 and Asp-81, Arg-66 and Asp-87,

and between His-283 and Asp-98. Interactions involving the loop between residues 283-301 are through hydrogen bonds between the main chain backbone amides of Gln-288 and Tyr-289, and the carbonyl oxygen atoms of Gly-91 and Lys-92, respectively. As a consequence of these two H bonds a "pseudo helix turn" is formed within the loop β2-α3 which interacts with the N-terminal end of helix α11. Finally, a salt bridge between His-283 and Asp-98 is equivalent to those observed in the structures of OTC´s from *P. aeruginosa* and *M. tuberculosis*.

Hexameric structure- Lh-cOTC is a homohexamer endowed with 32 point-group symmetry (**Fig. 3*A***). The oligomeric assembly is made up of two stacked trimers related by a two-fold symmetry axis. The concave faces of the trimers where the active sites are located, are solvent exposed in the hexamer, while the convex faces constitute the contacting interfaces between trimers. As one trimer is rotated 60º with respect to the other along the molecular three-fold symmetry axis, the hexamer displays an almost perfect hexagonal projection. The overall dimensions of the hexamer are 100 x 100 x 110 $Å^3$. Two distinct features of the interactions between trimers are evident: first, the observed contacting interfaces are formed between pairs of monomers, involving a network of monomer-to-monomer interactions, and second, these interfaces exhibit two-fold symmetry. The average value of the buried surface area at the interface between contacting monomers is relatively large (~1260 $Å^2$). Residues participating in these interactions are mainly contributed by the last eight residues of each monomer forming the central core of the interface, and also by the helix α1, loop α1– β1 and, to a lesser extent, by the first six N-terminal residues. As shown in **Fig. 3*B*** the main contacting interface between monomers is formed by the residues His-35, Tyr-28, Phe-32, Leu-338, Phe-339 and Ile-340. Whereas the side chains of Leu-338 and Ile-340 from both monomers form a central aliphatic cluster, the phenyl ring of Phe-339 ring packs perpendicular to those of His-35 and Phe-32 and parallel to Tyr-28. The centroid of the phenyl ring of Phe-339 is separated by distances of between 4.9 Å and 5.5 Å from the other aromatic ring, which is typical of aromatic-aromatic interactions (35). Conversely, polar interactions are also identified in this contacting interface: a salt bridge is formed between His-47 and Glu-50 (3.4 Å) together with hydrogen bonds between the NE2 atom from the His-35 side chain and the carbonyl oxygen atom of Asn-337 (2.9 Å), and between the NH2 atom of Arg-342 and the carbonyl oxygen atom of Val-343 (3.5 Å), respectively. It is interesting to note that residues participating in the above described hydrophobic interactions are specific for Lh-cOTC, with only Tyr-28 being present in human and *P. aeruginosa* OTC´s. Indeed, with the exception of human aOTC, the OTC´s of known 3D structure lack C-terminal segments analogous to that from Lh-cOTC, reinforcing the notion that the C-terminal end of Lh-cOTC is a key structural determinant of the hexameric assembly.

Oligomeric state of Lh-cOTC in solution- The oligomeric state of Lh-cOTC in solution has been studied by analytical gel-filtration chromatography and analytical ultracentrifugation (**Fig. 4**). The first approach, in conjunction with SDS-PAGE, indicates that Lh-cOTC exists in solution as a species of 230.6 ± 3.1 kDa (n=5), with subunits of ~40 kDa (**Fig. 4*A***). Subsequent analysis by sedimentation equilibrium analyses identified a unique molecular species with a molecular mass of 230.8 ± 24.0 kDa (**Fig. 4*B***), and a sedimentation velocity analysis carried out in the 0.22-1.10 mg/ml protein concentration range demonstrated that Lh-cOTC is a homogeneous species, with a sedimentation coefficient of 9.8 ± 0.4 S (*inset* **Fig. 4*B***). Therefore, our results are consistent with Lh-cOTC being a hexamer in solution (240.0 kDa, theoretical mass), in agreement with the crystallographic results.

It has been recently reported that trimeric aOTC from *M. tuberculosis* forms crystallographic pseudo hexamers within the asymmetric unit of orthorhombic crystals (18). Three dimensional comparisons against the Lh-cOTC hexamer reveal that the arrangement of interacting trimers is almost identical, however, *M. tuberculosis* aOTC pseudo hexamers lack the hydrophobic clusters between trimers (**Fig. 5**), reflecting the importance of these clusters in the stabilization of the Lh-cOTC hexamer in solution. To validate this hypothesis we have prepared and characterized a deletion mutant of Lh-cOTC which lacks the last six amino acid residues (Lh-$cOTC_{337}$). Activity measurements show that purified recombinant Lh-$cOTC_{337}$ (**Fig. 6**) is an active transcarbamylase and thus that the enzymatic machinery is intact and properly folded. Similarly to Lh-cOTC, Lh-$cOTC_{337}$ was analyzed by analytical gel-filtration chromatography. The results show that it behaves in solution as a mixture of two well defined species with molecular masses of 115,4 ± 2,4 kDa (n = 6) and 42,5 ± 2,5 kDa (n = 6), respectively,

with subunits of ~39 kDa as revealed by SDS-PAGE (**Fig. 6**). These results compare well with the theoretical masses expected for the trimeric (117,9 kDa) and monomeric (39,3 kDa) species, respectively. In addition, higher order soluble components eluting close to the void volume were observed, indicating that Lh-cOTC$_{337}$ is more prone to aggregate, a propensity which eventually precluded further detailed biophysical characterization. Importantly, only the putative trimeric species exhibits transcarbamylase activity (**Fig. 6**) which supports the notion of Lh-cOTC$_{337}$ being a catalytic trimer and not an unspecific self-association intermediate of monomers. It should be notice that molecular species compatible with hexameric assemblies were not detected, providing convincing evidence that the C-terminal region of Lh-cOTC plays a critical role in stabilizing the Lh-cOTC hexamer assembly in solution.

We believe that these results are noteworthy as they reveal that minor changes at the C-terminal end of a protein structure may underpin significant changes in its associative behavior. In turn, this highlights mechanisms of protein evolution whereby relatively small changes in primary structure within preexisting highly symmetric oligomeric species may yield the emergence of higher-order assemblies. In this regard, it has been demonstrated that interactions between large nonpolar side chains is an efficient means to introduce permanent contacts between subunits (36), which is precisely the scenario observed for Lh-cOTC and also for the dodecameric assembly of aOTC from *P. furiosus*, where the interface between trimers around a three-fold symmetry axis is mainly composed of large and hydrophobic residues (17). Finally, it is evident that the highly conserved monomeric architecture of OTC´s provides this family of enzymes with a versatile scaffold which facilitates self-assemble into different oligomeric species, namely, trimers, hexamers and dodecamers, and further it can be stated that the family of OTC´s is characterized by a pseudo-pleomorphism (37) i.e. the same monomeric scaffold may adopt different oligomeric assemblies.

Metal-binding site- The phased-model difference Fourier map of Lh-cOTC revealed a peak (~ 20 σ) located at the local three-fold symmetry axis of Lh-cOTC. This spherical bunch of electron density has been interpreted as a metal bound to the protein that was further identified as Ni by XFE and XANES measurements. Supporting evidence for Ni^{2+}-binding came from anomalous difference maps prepared with data recorded at the Ni-peak (7.484 keV) (**Fig. 7**). As the Lh-cOTC crystals were not grown in the presence of added metal ions, any such ion present in the structure must have been scavenged during the purification protocol. The B factor of the nickel ion is comparable with those of the surrounding atoms, indicating that the metal may have a high occupancy.

The inner-sphere coordination environment of the nickel bound to Lh-cOTC is shown in detail in **Fig. 7.** Each trimer of the Lh-cOTC assembly binds one nickel ion. The metal ion has three nitrogen ligands, contributed by the His-79 side chains, and three oxygen ligands from three ordered water molecules. They are arranged around the Ni^{2+} with an octahedral geometry. The coordination distances between the Ni^{2+} ion and coordinating groups varies as expected from 2.1 to 2.2 Å.

Previous biochemical studies have demonstrated metal binding to OTC´s, in particular, of zinc and cadmium ions (38, 39). Whereas in the first case it has been shown that one Zn^{2+} is bound per protein monomer of aOTC from *E. coli*, in the latter one 0.8 mol of cadmium is bound per trimer of rat aOTC. Taken together, these results suggest the existence of at least two distinct metal-binding modes within OTCs: a monomer-based binding mode and an intrinsically trimer-based binding mode. In this context, the model proposed for a Zn^{2+}-binding site located at the L-ornithine binding site of human aOTC (40), can be considered as a monomer-based binding mode, whereas the metal-binding site proposed herein for the nickel ion would represent a trimer-based binding mode. As expected for such a binding mode, it involves the participation of a structural element intrinsic to the trimeric assembly, i.e., the three-fold symmetry axis. In fact, it has been shown that the center of cyclic and dihedral oligomers with three-fold or higher symmetry provides competent environments for the binding of metals (34). It is interesting to note that while aOTC from *E. coli* lacks a homologous histidine residue potentially involved in metal-binding, this amino acid residue is strictly conserved in all OTC´s from vertebrate sources (**Fig. S1),** which may indicate the presence of homologous metal-binding sites in these enzymes. This particular structural result warrant further investigation

In summary, the structural analysis of Lh-cOTC combined with mutagenesis and biophysical data provide strong evidence that Lh-cOTC exists

as a hexameric assembly in solution, and that the C-terminal end of the protein is critical for the stabilization of this oligomer. Excision of the last six residues of the polypeptide chain generates a metastable mutant that behaves as a mixture of monomeric and trimeric species with only the latter exhibiting ornithine transcarbamylase activity. Furthermore, a metal-binding site has been identified for the first time in a member of the OTC family, but is presumably conserved in other enzymes from vertebrate sources. Further mutagenesis and crystallographic studies on Lh-cOTC have been initiated to characterize the specificity of metal-binding and the modulation of the oligomeric state of the protein, by dissecting the role of individual amino acid residues from the hydrophobic cores between trimers.

Acknowledgements- We thank the ESRF (Grenoble, France) for provision of synchrotron radiation facilities. In particular, we would like to thank Petra Pernot for assistance in using the beamline ID23-1. Financial support from the Ministerio de Educación y Ciencia (BFU2007-67404/BMC) and the Factoría de Cristalización (Consolider-Ingenio-2007) to J.M.M. is greatly appreciated. J.M.M. thanks Dr. Shi for kindly providing a sample of *N*-(phosphonacetyl)-L-ornithine (PALO).

REFERENCES

1. Stalon, V., Legrain, C., and Wiame, J. M. (1977) *Eur. J. Biochem.* **74**, 319-327
2. Haas, D., Evans, R., Mercenier, A., Simon, J. P., and Stalon, V. (1979) *J. Bacteriol.* **139**, 713-720
3. Baur, H., Tricot, C., Stalon, V., and Haas, D. (1990) *J. Biol. Chem.* **265**, 14728-14731
4. Tricot, C., Nguyen, V. T., and Stalon, V. (1993) *Eur. J. Biochem.* **221**, 555-561
5. Sainz, G., Tricot, C., Foray, M. F., Marion, D., Dideberg, O., and Stalon, V. (1998) *Eur. J. Biochem.* **251**, 528-533
6. Tricot, C., Villeret, V., Sainz, G., Dideberg, O., and Stalon, V. (1998) *J. Mol. Biol.* **283**, 695-704
7. Villeret, V., Tricot, C., Stalon, V., and Dideberg, O. (1995) *Proc. Natl. Acad. Sci. USA,* **92**, 10762-10766
8. Baur, H., Stalon, V., Falmagne, P., Lüthi, E., and Haas, D. (1987) *Eur. J. Biochem.* **166**, 111-117
9. Marcq, S., Díaz-Ruano, A., Charlier, P., Dideberg, O., Tricot, C., Piérard, A., and Stalon, V. (1991) *J. Mol. Biol.* **220**, 9-12
10. Nguyen, V. T., Baker, D. P., Tricot, C., Baur, H., Villeret, V., Dideberg, O., Gigot, D., Stalon, V., and Haas, D. (1996) *Eur. J. Biochem.* **236**, 283-293
11. Lipscomb, W. N. (1994) *Adv. Enzymol. Relat. Areas Mol. Biol* **68**, 67-152
12. Shi, D., Morizono, H., Ha, Y., Aoyagi, M., Tuchman, M., and Allewell, N. (1998) *J. Biol. Chem.* **273**, 34247-34254
13. Shi, D., Morizono, H., Aoyagi, M., Tuchman, M., and Allewell, N. (2000) *Proteins Struct., Funct. Genet.* **39**, 271-277
14. Jin, L., Seaton, B. A., and Head, J. F. (1997) *Nat. Struct. Biol.* **4**, 622-625
15. Ha, Y., McCann, M. T., Tuchman, M., and Allewell, N. (1997) *Proc. Natl., Acad. Sci. USA* **94**, 9550-9555
16. Langley, D. B., Templeton, M. D., Fields, B. A., Mitchell, R. E., and Collyer, C. A. (2000) *J. Biol. Chem.* **275**, 20012-20019
17. Villeret, V., Clantin, B., Tricot, C., Legrain, C., Roovers, M., Stalon, V., Glansdorff, N., and van Beeumen, J. (1998) *Proc. Natl. Acad. Sci. USA* **95**, 2801-2806
18. Sankaranarayanan, R., Cherney, M. M., Cherney, L. T., Garen, C.R., Moradian, F., and James, M. N. G. (2008) *J. Mol. Biol.* **375**, 1052-1063
19. de las Rivas, B., Rodríguez, H., Angulo, I., Muñoz, R., and Mancheño, J. M. (2007) *Acta Crystallogr Sect.F Struct. Biol. Cryst. Commun.* **63**, 563-567
20. de las Rivas, B., Curiel, J.A., Mancheño, J.M., and Muñoz, R. (2007). *Biotechnol. Prog.* 2**3**, 680-686
21. Arena, M. E., Manca de Nadra, M. C., and Muñoz, R. (2002) *Gene* 301, 61-66
22. Spector, L., and Jones, M. E. (1963) *Methods in Enzymology* **6**, 557-562
23. Laue, T. M., Shah, B. D., Ridgeway, T. M., and Pelletier, S. L. (1992) *Biochemistry and Polymer Science* .Royal Society of Chemistry, London.
24. Solé, V. A., Papillon, E., Cotte, M., Walter, Ph., and Susini, J. (2007) *Spectrochim. Acta B* **62,** 63-68
25. Leslie, A.G.W. (1992) *Joint CCP4 + ESF-EAMCB Newsletter on Protein Crystallography* **26**
26. Collaborative Computational Project, Number 4. (1994) *Acta Crystallogr. Sect. D Biol. Crystallogr.* **50**, 760-763
27. Vagin, A., and Teplyakov, A. (1997) *J. Appl. Crystallogr.* **30**, 1022-1025
28. Murshudov, G. N., Vagin, A. A., and Dobson, E. J. (1997) *Acta Crystallogr. Sect. D Biol. Crystallogr.* 53, 240-255
29. Perrakis, A., Morris, R., and Lamzib, V.S. (1999) *Nat. Struct. Biol.* **6**, 458-463
30. Jones, T. A., Zou, J-Y., Cowtan, S. W., and Kjelgaard, M. (1991) *Acta Crystallog. Sect. A* **47**, 110-119
31. Laskowski, R., MacArthur, M., Moss, D., and Thornton, J. M. (1993) *J. Appl. Crystallogr.* 26, 283–291
32. Kabsch, W. (1976) *Acta Crystallogr. Sect. A.* **32**, 922-923
33. Krissinel, E., and Henrick, K. (2007) *J. Mol. Biol.* **372**, 774-797
34. DeLano, W.L. The PyMOL Molecular Graphics System (2002) DeLano Scientific, Palo Alto, CA, USA.

35. Burley, S. K., and Petsko, G.A. (1985) *Science* **229**, 23-28
36.Grueninger, D., Treiber, N., Ziegler, M. O. P., Koetter, J. W. A., Schulze, M. S., and Schulz, G. E. (2008) *Science* **319**, 206-209
37. Goodsell, D. S., and Olson, A. J. (2000) *Annu. Rev. Biophys. Biomol. Struct.* **29**, 105-153
38. Kuo, L. C., Caron, C., Lee, S., and Herzberg, W. (1990) *J. Mol. Biol.* **211**, 271-280
39. Aoki, Y., Sunaga, H., and Suzuki, K. T. (1988) *Biochem. J.* **250**, 735-742
40. Shi, D., Morizono, H., Yu, X., Tong, L., Allewell, N. M., and Tuchman, M. (2001) *Biochem. J.* **354**, 501-509

FOOTNOTES

*This work was supported by the Ministerio de Ciencia e Innovación, BFU2007-67404/BMC (to J. M. M.), and the "Factoría de Cristalización" Consolider-Ingenio-2007 (to J.M.M.), AGL2008-001052 (to R. M.), FUN-C-FOOD Consolider 25506 (to R. M.), and Comunidad de Madrid S-0505/AGR/000153 (to R. M.). H. R. is a recipient of an I3P predoctoral fellowship from the CSIC.

The atomic coordinates and structure factors (code 2W37) *have been deposited in the Protein Data Bank, Research Collaboratory for Structural Bioinformatics, Rutgers University, New Brunswick, NJ (http://www.rcsb.org/).*

§Present address: The Scripps Research Institute, Scripps Florida, Jupiter, FL, USA.

[1]The abbreviations used are: CP, carbamoyl phosphate; Lh-cOTC, *Lactobacillus hilgardii* catabolic ornithine transcarbamylase; L-NVA, L-norvaline; ORN, ornithine; PALO, *N*-(phosphonacetyl)-L-ornithine;

FIGURE LEGENDS

FIGURE 1. **Three dimensional structure of the monomeric subunit of Lh-cOTC.** *Ribbon model* of the crystal structure with secondary structural elements colored *blue* for β-strands, *orange* for α-helix, and *green* for regions with no regular secondary structure. The secondary structural assignments as well as the N and C termini of the model are shown. The figure was prepared with PyMol (34).

FIGURE 2. **Sequence alignment of Lh-cOTC with other OTC and *E. coli* ATC sequences.** The secondary structural elements of Lh-cOTC are shown as *green cylinders* (α-helix) and *orange arrows* (β-strand). Invariant residues are in *blue*, and those highly conserved are shown in *yellow*.

FIGURE 3. **Overall views of the crystal structure of the Lh-cOTC hexamer and main interactions identified at the contacting interface between trimers**. Ribbon diagram of the Lh-cOTC hexamer (*A*). *Top left*, Lh-cOTC viewed parallel to the molecular three-fold symmetry axis; *top right*, side-view of the hexamer perpendicular to the two-fold symmetry axis. Each trimer is represented by a different color. The Ni^{2+} ions are indicated by *orange spheres.* Stereoview of the contacting interface between monomers from different trimers (*B*). The main residues shaping the hydrophobic cores are shown in *stick representation*: Tyr-28, Phe-32, His-35, Leu-338, Phe-339 and Ile-340.

FIGURE 4. **Characterization of the oligomeric state of Lh-cOTC in solution.** Analytical equilibrium ultracentrifugation analysis of Lh-cOTC (20.5 μM) at 12,000 rpm (*A*). Absorbance at 280 nm is plotted against the radial position from the center of the rotor (*open circles*). The best fit to the data set (*solid line*) corresponds to a unique species of molecular mass 230.8 ± 24.0 kDa. Residuals from this fit are shown in panel *B*. Sedimentation velocity analysis of Lh-cOTC (20.5 μM) at 45,000 rpm (*inset panel A*) reveals the presence of a homogeneous species with a sedimentation coefficient 9.8 ± 0.4 S. *C*, analytical gel filtration studies of Lh-cOTC on Superdex 75 10/300 GL. The elution profile of Lh-cOTC (80 μg) is shown together with the elution positions of some standard proteins (thyroglobulin, 667 kDa; IgG, 158 kDa; ovalbumin, 43 kDa; myoglobin, 17 kDa; vitamin B12, 1.3 kDa). The void volume elutes at 8.3 min. The scale at the *bottom* indicates the elution time. *Inset*, semilog plot of the molecular mass of all the standard proteins used *versus* their K_{av} values. The results indicate that Lh-cOTC has a molecular mass of 230.6 ± 3.1 kDa (*closed circle*).

FIGURE 5. **Contacting interfaces between monomers from different trimers in Lh-cOTC and aOTC from *M. tuberculosis.*** Ribbon diagram representation of contacting monomers from different trimers in Lh-cOTC (*A*) and in aOTC from *M. tuberculosis* (*B*) (PDB entry: 2P2G). The region shown in this figure is the same presented in figure 3*B*. In both enzymes, contacting monomers from different trimers are shown in *blue* and *orange*, respectively. Comparison of the two crystal structures reveals an r.m.s.d. value of 1.2 Å for 285 aligned C_α atoms.

FIGURE 6. **Purification and oligomeric state of the Lh-cOTC$_{337}$ mutant.** *A*, absorbance profile at 280 nm of the HisTrap FF Ni-affinity column eluate (*solid line*). The eluted fractions were tested for their transcarbamylase activity (*open circles* and *dashed line*) and also for their content of Lh-cOTC$_{337}$ by SDS-PAGE (*inset*). From left to right, lanes correspond to even fractions from 2 to 20, and to molecular mass markers. *B*, analytical gel filtration studies of Lh-cOTC$_{337}$ using a Superdex 75 10/300 GL column. Fractions 10 to 14 were analyzed separately with a Superdex 75 10/300 GL, showing identical normalized absorbance profiles at 280 nm (*solid line*). As above, eluted fractions were evaluated for their transcarbamylase activity (*open circles* and *dashed line*). The indicated elution positions of standard proteins are the same as in figure 4*C*.

FIGURE 7. **Ni^{2+} binding by Lh-cOTC.** *A*, a stereo view representation of the Ni^{2+} binding site. Histidine residues that form the inner-sphere contacts with the Ni^{2+} ion (*yellow sphere*) are shown as *sticks;* nitrogen atoms are *blue* and oxygen atoms are *red*. Three coordinating water molecules are shown as *red balls*. Glutamic acid residues that directly interact with the water molecules are also indicated. Superposed on this final model are two electron density maps, a 2.1-Å $2F_o - F_c$ map from the Lh-cOTC

structure contoured at the 1-σ level (*orange*), and an anomalous difference map prepared with data recorded at the Ni2+ peak (7.484 keV) contoured at the 4-σ level (*green*). *B*, further details of the binding site. Distances are given in Å.

Table 1.
Data collection and refinement statistics
Values in parentheses are for the highest resolution shell.

PDB code	2W37
Data collection	
Beamline	BM16 (ESRF)
Space group	*P*321
Unit cell parameters (Å)	
	a = 156.80
	b = 156.80
	c = 80.62
V_M (Å^3/Da)	2.56
Solvent content (%, v/v)	51.9
Wavelength (Å)	0.977
Resolution range (Å)	78-2.10 (2.21-2.10)
Completeness (%)	95.8 (95.8)
Unique reflections	63810
Multiplicity	5.2 (2.5)
R_{merge} (%)	8.8 (47.4)
Average I/σ	13.8 (1.7)
Molecules/asymmetric unit	3
Wilson B (Å^2)	32.7
Refinement	
Resolution range (Å)	69-2.10
R_{work} (%)	19.8
R_{free} (%)	24.4
Number of atoms	
Protein	8031
Waters	341
Ni^{2+}	1
Geometry statistics	
R.m.s. deviations, bonds (Å)	0.012
R.m.s. deviations, angles (º)	1.3
Ramachandran Plot	
Most favored (%)	90.0
Allowed (%)	9.7
Disallowed (%)	0.3

Table 2.
Hydrogen bonding interactions and salt bridges identified in the interface between monomers inside the trimers.

Atoms monomer 1	Atoms monomer 2	Distance (Å)
Ser-61 OG*	Asn-86 O	3.4
Thr-63 OG1*	Asp-87 O	3.5
Arg-64 NH1§	Glu-94 OE1	3.7
Arg-64 NH2§	Glu-94 OE1	2.8
Arg-64 NH2§	Glu-94 OE2	3.3
Arg-66 NE§	Glu-81 OE2	3.4
Arg-66 NH1§	Asp-87 OD2	3.7
Arg-66 NH1§	Asp-87 OD1	3.6
Arg-66 NH2*	Tyr-82 O	2.9
Arg-66 NH2§	Glu-81 OE2	2.9
Ser-67 OG*	Glu-81 OE1	2.7
Thr-71 O	Asn-53 ND2*	3.7
Asp-75 OD1	Asn-53 ND2*	3.2
Tyr-82 OH*	Asp-87 OD1	3.7
His-283 NE2§	Asp-98 OD1	3.4
His-283 NE2§	Asp-98 OD2	2.7
Gln-288 OE1	Lys-92 NZ*	3.7
Gln-288 N*	Gly-91 O	3.0
Gln-288 N*	Lys-92 O	3.7
Tyr-289 N*	Lys-90 O	3.4
Tyr-289 N*	Lys-92 O	3.2

* Hydrogen bond donor.
§ The cation of the salt bridge.

FIGURE 1

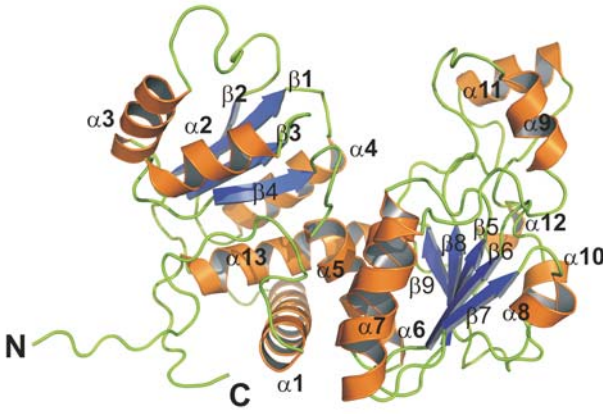
α3
α2
β2
β1
β3
α4
β4
α13
α5
α7
α6
α1
N
C
α11
α9
β5
α12
β8
β6
α10
β9
β7
α8

Figure 2

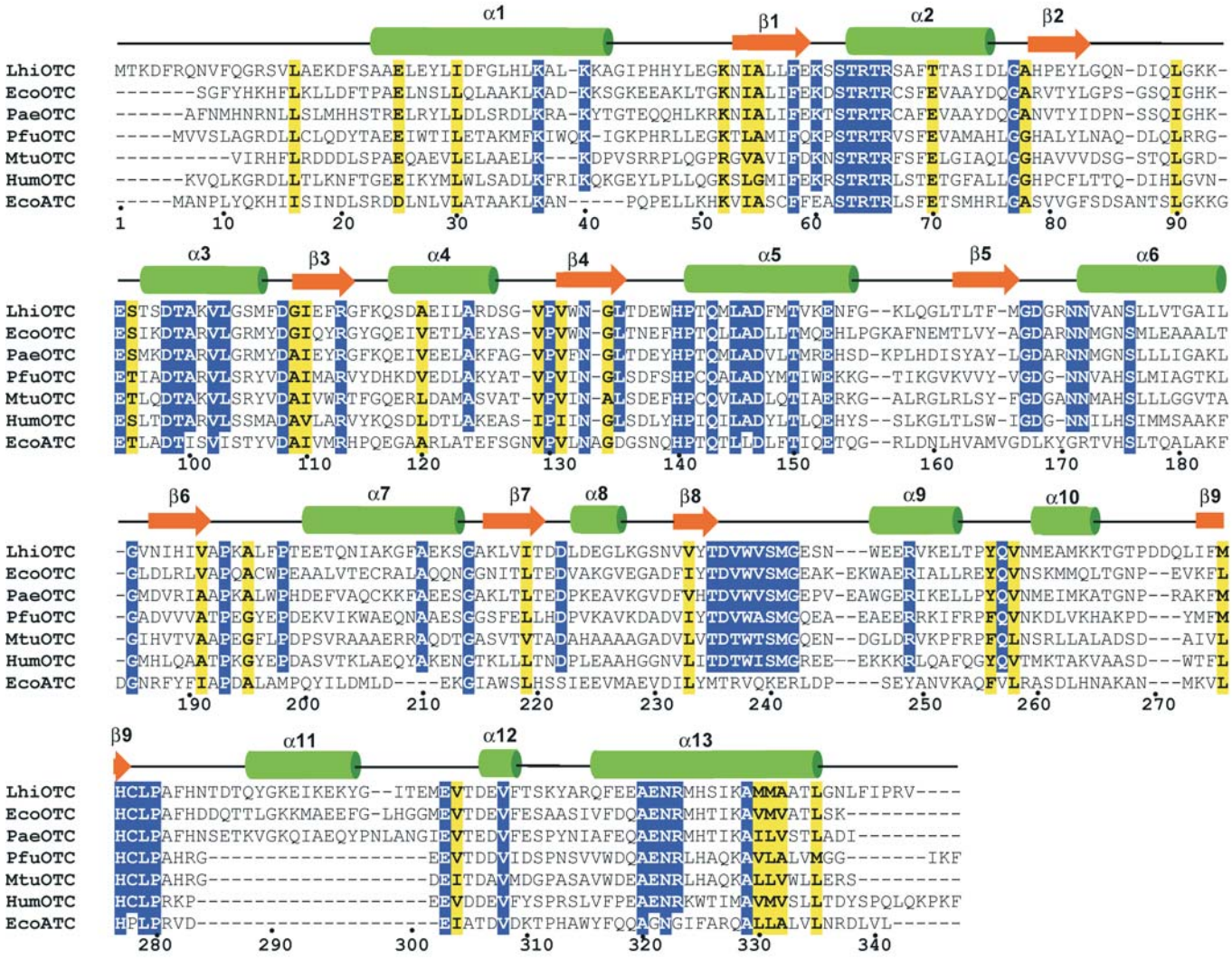
α1
β1
α2
β2
LhiOTC MTKDFRQNVFQGRSVLAEKDFSAAELEYLIDFGLHLKALKKAGIPHHYLEGKNIALLFEKSSTRTRSAFTTASIDLGAHPEYLGQN-DIQLGKK-
EcoOTC -------SGFYHKHFLKLLDFTPAELNSLLQLAAKLKADKKSGKEEAKLTGKNIALIFEKDSTRTRCSFEVAAYDQGARVTYLGPS-GSQIGHK-
PaeOTC ------AFNMHNRNLLSLMHHSTRELRYLLDLSRDLKRAKYTGTEQQHLKRKNIALIFEKTSTRTRCAFEVAAYDQGANVTYIDPN-SSQIGHK-
PfuOTC -----MVVSLAGRDLLCLQDYTAEEIWTILETAKMFKIWQK-IGKPHRLLEGKTLAMIFQKPSTRTRVSFEVAMAHLGGHALYLNAQ-DLQLRRG-
MtuOTC ----------VIRHFLRDDDLSPAEQAEVLELAAELK---KDPVSRRPLQGPRGVAVIFDKNSTRTRFSFELGIAQLGGHAVVVDSG-STQLGRD-
HumOTC ------KVQLKGRDLLTLKNFTGEEIKYMLWLSADLKFRIKQKGEYLPLLQGKSLGMIFEKRSTRTRLSTETGFALLGGHPCFLTTQ-DIHLGVN-
EcoATC -----MANPLYQKHIISINDLSRDDLNLVLATAAKLKAN-----PQPELLKHKVIASCFFEASTRTRLSFETSMHRLGASVVGFSDSANTSLGKKG
1 10 20 30 40 50 60 70 80 90
α3
β3
α4
β4
α5
β5
α6
LhiOTC ESTSDTAKVLGSMFDGIEFRGFKQSDAEILARDSG-VEVWN-GLTDEWHPTQMLADFMTVKENFG--KLQGLTLTF-MGDGRNNVANSLLVTGAIL
EcoOTC ESIKDTARVLGRMYDGIQYRGYGQEIVETLAEYAS-VEVWN-GLTNEFHPTQLLADLLTMQEHLPGKAFNEMTLVY-AGDARNNMGNSMLEAAALT
PaeOTC ESMKDTARVLGRMYDAIEYRGFKQEIVEELAKFAG-VEVFN-GLTDEYHPTQMLADVLTMREHSD-KPLHDISYAY-LGDARNNMGNSLLLIGAKL
PfuOTC ETIADTARVLSRYVDAIMARVYDHKDVEDLAKYAT-VEVIN-GLSDFSHPCQALADYMTIWEKKG--TIKGVKVVY-VGDG-NNVAHSLMIAGTKL
MtuOTC ETLQDTAKVLSRYVDAIVWRTFGQERLDAMASVAT-VEVIN-ALSDEFHECQVLADLQTIAERKG--ALRGLRLSY-FGDGANNMAHSLLLGGVTA
HumOTC ESLTDTARVLSSMADAVLARVYKQSDLDTLAKEAS-IPIIN-GLSDLYHPIQILADYLTLQEHYS--SLKGLTLSW-IGDG-NNILHSIMMSAAKF
EcoATC ETLADTISVISTYVDAIVMRHPQEGAARLATEFSGNVEVLNAGDGSNQHPTQTLLDLFTIQETQG--RLDNLHVAMVGDLKYGRTVHSLTQALAKF
100 110 120 130 140 150 160 170 180
β6
α7
β7
α8
β8
α9
α10
β9
LhiOTC -GVNIHIVAPKALEPTEETQNIAKGPAEKSGAKLVITDDLDEGLKGSNVVYTDVWVSMGESN---WEERVKELTPYQVNMEAMKKTGTPDDQLIFM
EcoOTC -GLDLRLVAPQACWPEAALVTECRALAQQNGGNITLTEDVAKGVEGADFIYTDVWVSMGEAK-EKWAERIALLREYQVNSKMMQLTGNP--EVKFL
PaeOTC -GMDVRIAAPKALWPHDEFVAQCKKPAEESGAKLTLTEDPKEAVKGVDFVHTDVWVSMGEPV-EAWGERIKELLPYQVNMEIMKATGNP--RAKFM
PfuOTC -GADVVVATPEGYEPDEKVIKWAEQNAAESGGSFELLHDPVKAVKDADVIYTDVWASMGQEA--EAEERRKIFRPFQVNKDLVKHAKPD---YMFM
MtuOTC -GIHVTVAAPEGFLPDPSVRAAAERRAQDTGASVTVTADAHAAAAGADVLVTDTWTSMGQEN--DGLDRVKPFRPFQLNSRLLALADSD---AIVL
HumOTC -GMHLQAATPKGYEPDASVTKLAEQYAKENGTKLLLTNDPLEAAHGGNVLITDTWISMGREE--EKKKRLQAFQGYQVTMKTAKVAASD---WTFL
EcoATC DGNRFYFIAPDALAMPQYILDMLD----EKGIAWSLHSSIEEVMAEVDILYMTRVQKERLDP----SEYANVKAQFVLRASDLHNAKAN---MKVL
190 200 210 220 230 240 250 260 270
β9
α11
α12
α13
LhiOTC HCLPAFHNTDTQYGKEIKEKYG--ITEMEVTDEVFTSKYARQFEEAENRMHSIKAMMAATLGNLFIPRV----
EcoOTC HCLPAFHDDQTTLGKKMAEEFG-LHGGMEVTDEVFESAASIVFDQAENRMHTIKAVMVATLSK----------
PaeOTC HCLPAFHNSETKVGKQIAEQYPNLANGIEVTEDVFESPYNIAFEQAENRMHTIKAILVSTLADI---------
PfuOTC HCLPAHRG-------------------EEVTDDVIDSPNSVVWDQAENRLHAQKAVLALVMGG-------IKF
MtuOTC HCLPAHRG-------------------DEITDAVMDGPASAVWDEAENRLHAQKALLVWLLERS---------
HumOTC HCLPRKP-------------------EEVDDEVFYSPRSLVFPEAENRKWTIMAVMVSLLTDYSPQLQKPKF
EcoATC HPLPRVD-------------------EIATDVDKTPHAWYFQQAGNGIFARQALLALVLNRDLVL------
280 290 300 310 320 330 340

FIGURE 3

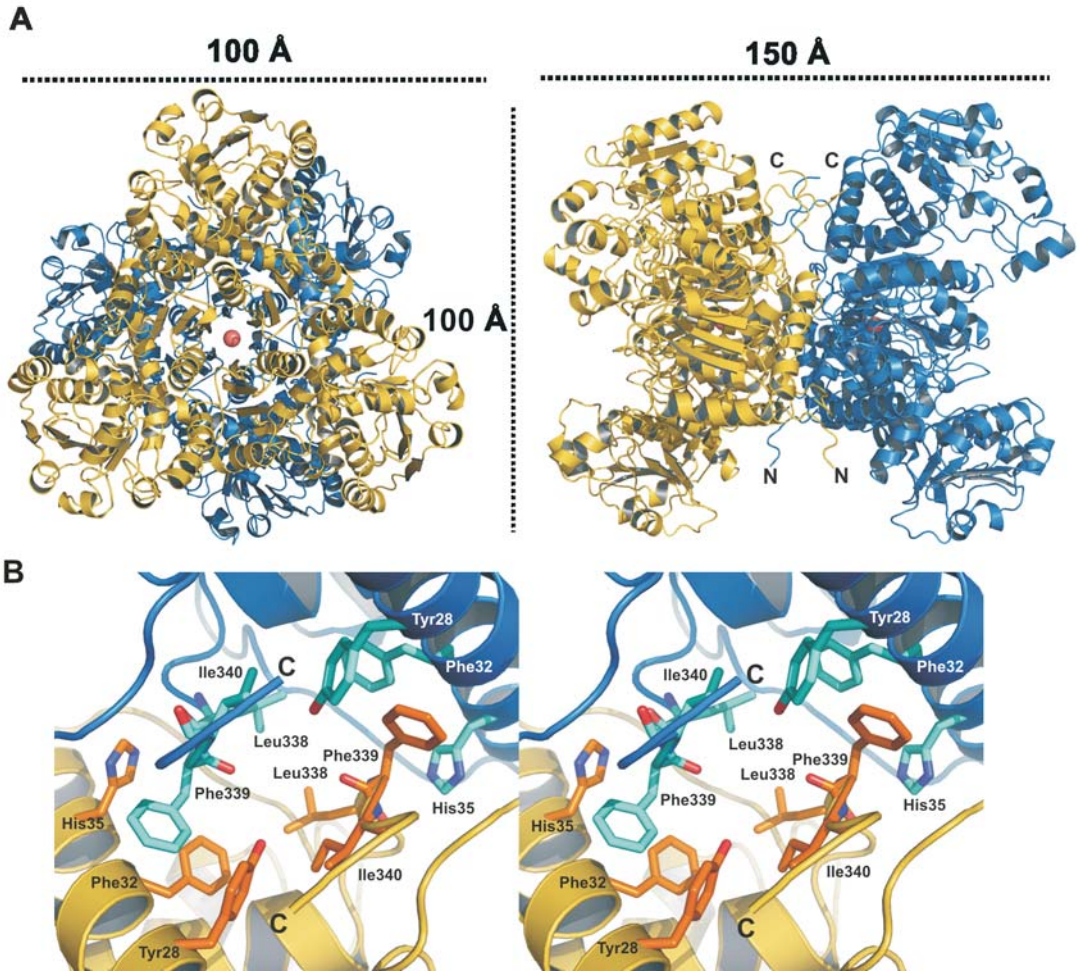
A
100 Å
150 Å
100 Å
C
C
N
N
B
Tyr28
Phe32
Ile340
C
Leu338
Phe339
Leu338
Phe339
His35
His35
Phe32
Ile340
C
Tyr28
Tyr28
Phe32
Ile340
C
Leu338
Phe339
Leu338
Phe339
His35
His35
Phe32
Ile340
C
Tyr28

FIGURE 4

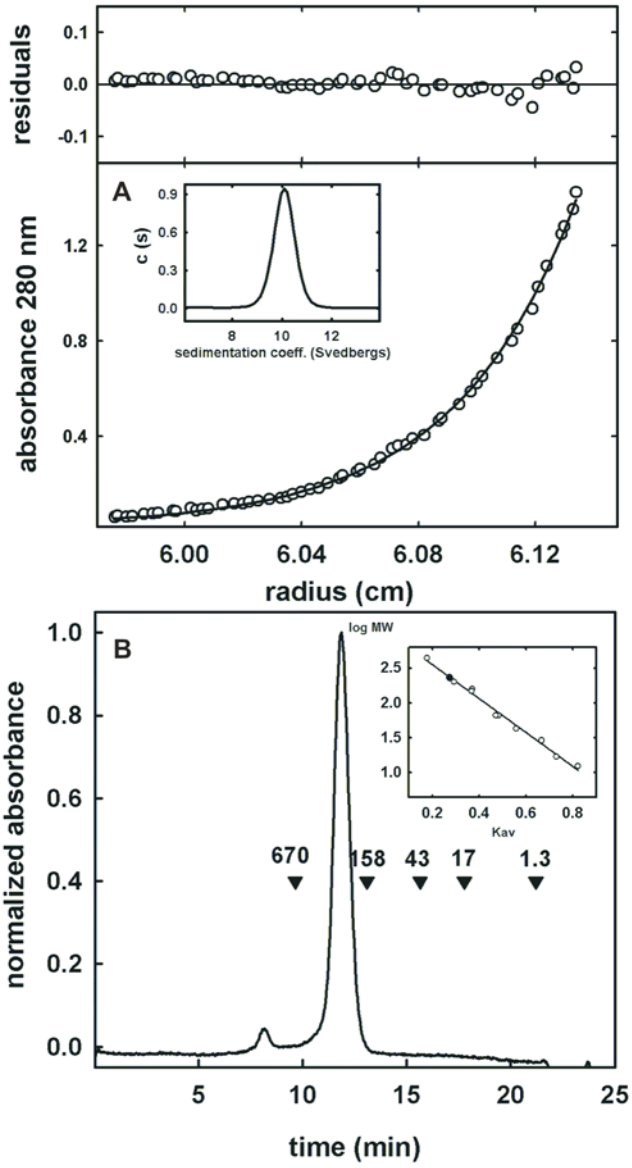
residuals
0.1
0.0
-0.1
A
absorbance 280 nm
1.2
0.8
0.4
c (s)
0.9
0.6
0.3
0.0
8
10
12
sedimentation coeff. (Svedbergs)
6.00
6.04
6.08
6.12
radius (cm)
B
normalized absorbance
1.0
0.8
0.6
0.4
0.2
0.0
log MW
2.5
2.0
1.5
1.0
0.2
0.4
0.6
0.8
Kav
670
158
43
17
1.3
5
10
15
20
25
time (min)

FIGURE 5

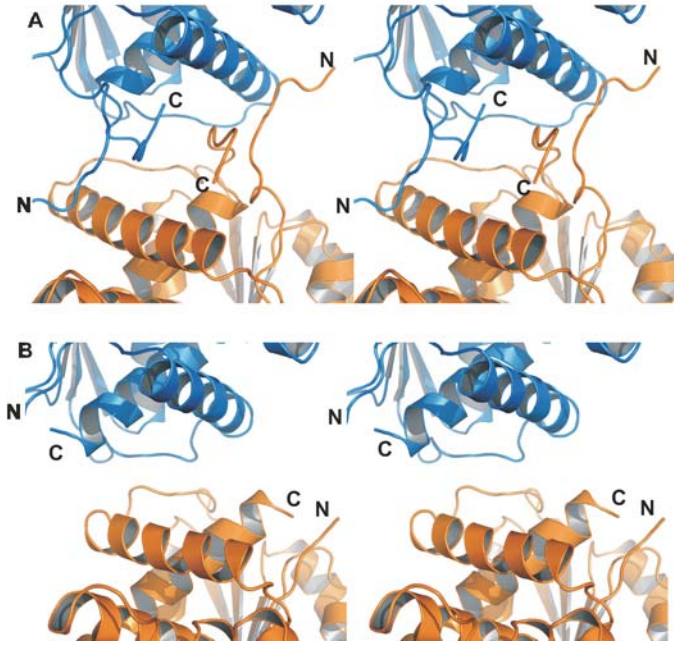

FIGURE 6

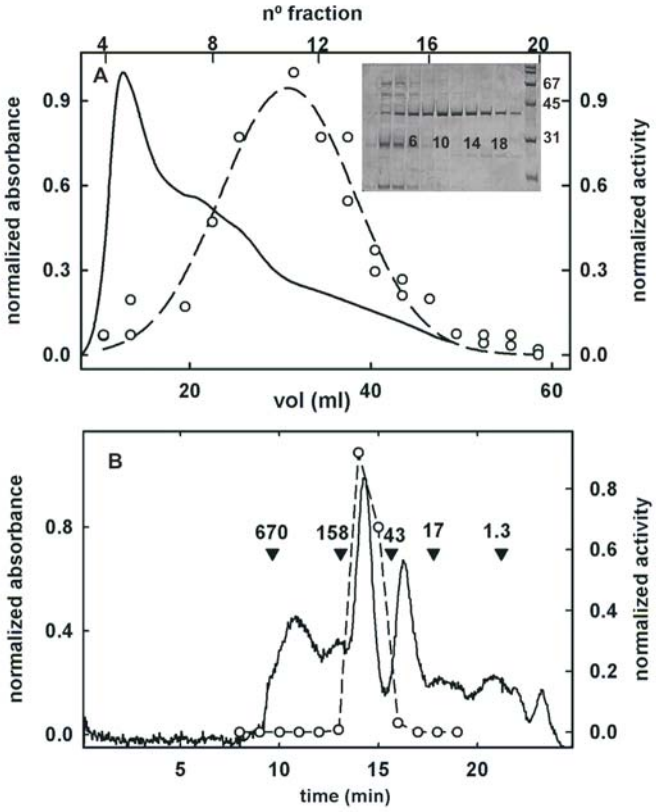
nº fraction
4
8
12
16
20
A
normalized absorbance
normalized activity
0.0
0.3
0.6
0.9
67
45
31
6
10
14
18
20
40
60
vol (ml)
B
670
158
43
17
1.3
0.0
0.4
0.8
0.2
0.6
5
10
15
20
time (min)

FIGURE 7

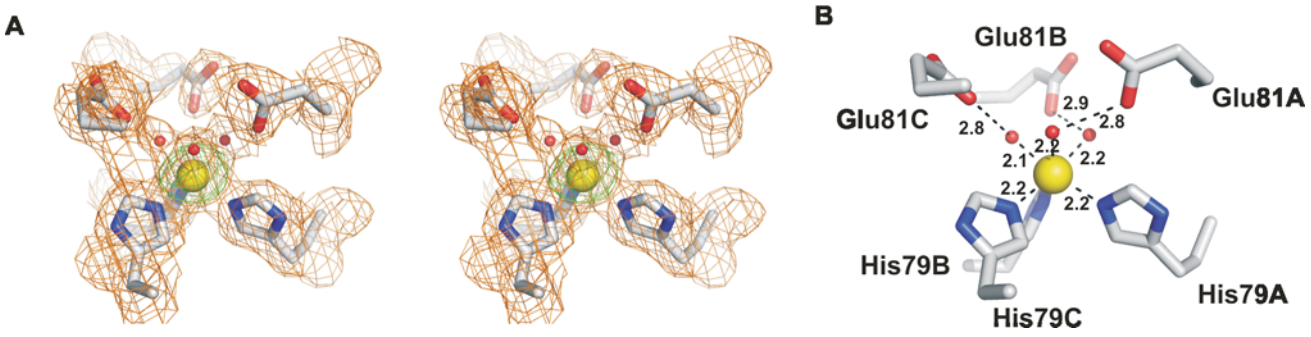
A
B
Glu81B
Glu81A
Glu81C
2.9
2.8
2.8
2.9
2.1
2.2
2.2
2.2
His79B
His79A
His79C